

## Research papers

# Sensitivity analysis and calibration for a two-dimensional state-space model of metal hydride storage tanks based on experimental data

Mingrui Chen<sup>a</sup>, Carles Batlle<sup>b</sup>, Bryan Escachx<sup>a</sup>, Ramon Costa-Castelló<sup>e,\*</sup>, Jing Na<sup>c,d</sup>

<sup>a</sup> Institut de Robòtica i Informàtica Industrial, CSIC-UPC. C/ Llorens i Artigas 4-6, 08028 Barcelona, Spain

<sup>b</sup> Departament de Matemàtiques, Institut d'Organització i Control, EPSEVG, UPC, 08800 Vilanova i la Geltru, Spain

<sup>c</sup> Faculty of Mechanical and Electrical Engineering, Kunming University of Science and Technology, Kunming, 650500, PR China

<sup>d</sup> Yunnan Key Laboratory of Intelligent Control and Application, Kunming, 650500, PR China

<sup>e</sup> Universitat Politècnica de Catalunya (UPC). Escola Tècnica Superior d'Enginyeria Industrial de Barcelona (ETSEIB), Av. Diagonal 647, 2, 08028 Barcelona, Spain



## ARTICLE INFO

## Keywords:

Metal hydride tanks  
Mathematical model  
Sensitivity analysis  
Model calibration  
Temperature sensors  
Particle swarm optimization

## ABSTRACT

In this paper, a state-space model of a metal hydride tank is formulated and analyzed in detail. Firstly, a three-dimensional state-space model of the metal hydride tank is simplified by assuming that the tank temperature can be measured. Secondly, the model is completed with a pipe model, which allows to compute the input flow from the pipe pressure that can be easily measured. The proposed model solves the problem that the conventional metal hydride tank models usually take the mass flow rate as input and ignore the pressure as system input. Thirdly, the first-order trajectory sensitivity analysis method is adopted to determine the sensitivity of selected unknown parameters. Latter, the particle swarm optimization algorithm is used to estimate the unknown model parameters from experimental data. Finally, a comparison between experimental data and simulation results demonstrates that the proposed model can reflect the dynamic characteristics of the metal hydride tank.

## 1. Introduction

To overcome the intermittency of renewable energy sources, energy storage systems and thermal management strategies are receiving increasing attention [1,2]. Hydrogen is considered an attractive and sustainable energy carrier due to its eco-friendly and high-energy density characteristics [3]. There are three main methods used to store hydrogen: compressed gas, cryogenic liquid hydrogen, and solid-state storage methods [4]. Solid-state hydrogen storage has a broad development prospect compared to the other two types of hydrogen storage due to its ability to store large amounts of hydrogen in a small volume with negligible leakage. The metal hydride (MH) tank is one type of container for solid-state hydrogen storage. However, modeling of the MH tank remains a challenge that has not been fully solved.

Physical modeling of the MH tank started earlier in the 1980s. Suda et al. [5] studied the reaction kinetics of metal hydrides and their mixtures in the absorption and desorption processes, and they obtained the reaction kinetic expressions for these two processes based on experiments. Nishizaki et al. [6] proposed a model for calculating the coefficients of performance, and they used an equation that included the equilibrium pressure to fit the pressure-composition-temperature

(PCT) curve obtained from the experiment. These studies have provided a basis for the modeling of MH tanks, but these models only address partial properties of the MH tank. A one-dimension mathematical model containing both transient heat and mass transfer of MH reaction beds was presented by Mayer et al. [7]. The heat conduction equations and the mass diffusion equation for a cylindrical MH reaction bed in longitudinal and radial directions are studied in their work. An assumption was used that the length of a cylindrical reaction bed is longer than its diameter so that heat conduction can be considered to be in the radial direction only. Jemni and Nasrallah et al. [8,9] proposed a two-dimensional model of the MH tank where the modified expressions proposed for the reaction kinetics have been adopted by a large number of subsequent researchers. In addition, they also modified the Van't Hoff equation: the standard Van't Hoff equation could not be applied for different hydrogen-to-metal atomic ratios (H/M), so some terms including H/M were introduced into the Van't Hoff equation and a 5-order polynomial was used to calculate the equilibrium pressure. Then in [10], they used the Arrhenius equation to fit the experimental data obtained, and the results showed a good fit to the experimental

\* Corresponding author.

E-mail addresses: [chenmingrui2018@gmail.com](mailto:chenmingrui2018@gmail.com) (M. Chen), [carles.batlle@upc.edu](mailto:carles.batlle@upc.edu) (C. Batlle), [bryan.escachx@upc.edu](mailto:bryan.escachx@upc.edu) (B. Escachx), [ramon.costa@upc.edu](mailto:ramon.costa@upc.edu) (R. Costa-Castelló), [najing25@163.com](mailto:najing25@163.com) (J. Na).

<https://doi.org/10.1016/j.est.2024.112316>

Received 5 March 2024; Received in revised form 4 May 2024; Accepted 26 May 2024

Available online 12 June 2024

2352-152X/© 2024 The Author(s). Published by Elsevier Ltd. This is an open access article under the CC BY-NC license (<http://creativecommons.org/licenses/by-nc/4.0/>).

**Nomenclature****Abbreviations**

MH	Metal hydride
PCT	Pressure-Composition-Temperature
FOTSA	First-order Trajectory Sensitivity Analysis
FOTSF	First-order Trajectory Sensitivity Function
SOC	State of charge

**Parameters**

$\rho_g$	Density of hydrogen (kg/m <sup>3</sup> )
$m'_{in}$	Mass rate of hydrogen (kg/s)
$m'_r$	Mass rate of hydrogen sorption (kg/s)
$V_{tank}$	Volume of tank (m <sup>3</sup> )
$V_{MH}$	Volume of MH (m <sup>3</sup> )
$\epsilon$	Porosity of MH
$f_{in}$	Normalized mass flow rate of hydrogen (kg/m <sup>3</sup> /s)
$f_r$	Normalized sorption mass flow rate of hydrogen (kg/m <sup>3</sup> /s)
$V_g$	Normalized volume of hydrogen
$\rho_s$	Density of the MH (kg/m <sup>3</sup> )
$V_s$	Normalized volume of the MH
$C_a$	Absorption constant (1/s)
$C_d$	Desorption constant (1/s)
$E_a$	Activation energy of absorption (J/mol)
$E_d$	Activation energy of desorption (J/mol)
$P_{eq,a}$	Equilibrium pressure of absorption (Pa)
$P_{eq,d}$	Equilibrium pressure of desorption (Pa)
$R$	Universal gas constant (8.314 J/mol/K)
$m_{H_2,c}$	Capacity of hydrogen absorption (kg)
$\rho_{ss}$	Saturated density of MH with complete absorption of hydrogen (kg/m <sup>3</sup> )
$\rho_{s0}$	Empty density of the MH without any hydrogen (kg/m <sup>3</sup> )
$P$	Pressure of hydrogen (Pa)
$M_{H_2}$	Molar mass of hydrogen (2.016 × 10 <sup>-3</sup> kg/mol)
$V_{H_2}$	Maximum volume of hydrogen that can be absorbed (m <sup>3</sup> )
$\rho_{H_2}$	Density of hydrogen in standard state (kg/m <sup>3</sup> )
$P_0$	Atmospheric pressure (101 325 Pa)
$\Delta S_d$	Entropy change for desorption (J/mol/K)
$\Delta H_d$	Enthalpy change for desorption (J/mol)
$\varphi, \varphi_0$	Plateau flatness coefficients
$\beta$	Plateau hysteresis coefficient
$F_{in}$	Flow rate of hydrogen (Ln/min)
$P_{pipe}$	Pressure of pipe (Pa)
$wt$	Mass percentage of hydrogen relative to alloy (%)
$Q$	Heat exchange per unit volume from the ambient air to the MH tank (W/m <sup>3</sup> )
$C_{ps}$	Specific heat of hydrogen (J/(kg K))

$C_{ps}$  Specific heat of MH (J/(kg K))

**Subscripts**

$a$	Absorption
$d$	Desorption

data under different conditions. A three-dimensional model of the MH tank was proposed by Aldas et al. [11]. The internal metal of the MH tank used in the experiment was LaNi<sub>5</sub> and they studied the processes of heat and mass transfer, fluid flow and chemical reaction in different directions.

Subsequently, since the physical modeling of the MH tank was difficult due to its strong nonlinearity and a large number of unknown internal parameters, some researchers adopted a black-box model for the MH tank. Stark et al. [12] combined neural networks with fuzzy techniques to develop a neural-network-based model of the MH tank. To train the neural network, externally accessible parameters that could be obtained from measurements, such as storage pressure, ambient temperature and hydrogen flow rate were used. Because of the large differences between the absorption and desorption processes in the MH tank, they built two identically structured, but individually parameterized models.

The models developed in the above literature have a common feature of containing a large number of parameters and variables. While some of these variables can be measured directly by sensors, e.g. the pressure in the MH tank can be obtained by pressure sensors, and the mass flow rate can be obtained by flow meters, a majority of the parameters cannot be directly measured. Consequently, in practical research, how to calibrate the unknown parameters in the model based on experimental data is also a question worthy of attention. Optimization algorithms are one of the essential methods for model calibration. The main idea of the optimization algorithm is to adjust the unknown parameters so that a suitable cost function is minimized [13,14]. Intelligent optimization algorithms can be applied to search for the optimal solution of unknown parameters. The commonly used intelligent optimization algorithms mainly include genetic algorithm (GA) [15,16], ant colony algorithm (ACO) [17] and particle swarm optimization (PSO) algorithm [18]. Zhu et al. [19] identified unknown parameters in the MH tank model of the onboard hydrogen storage system through the PSO algorithm. The unknown parameters were set as particles, and the fitness function was defined as the root mean square error between the model simulation result and actual experimental data. The PSO algorithm was then executed, and the final optimal positions of the particles were adopted as the identified values for the unknown parameters. Experimental results showed that the maximum error between the simulation and the actual system was less than 9%. For the same purpose, Suárez et al. [20] used the PSO algorithm to estimate the uncertain physical parameters in the model and subsequently used the calibrated model to study degradations in the MH tanks.

To the best of our knowledge, in most mathematical models of MH tanks, it is common to consider the mass flow rate as a known quantity to establish the mass balance equations. However, a working condition that is rarely considered in the literature is the behavior of charging and discharging controlled by external pipe pressure. Motivated by this fact, in this paper, a pipe model is introduced to calculate the mass flow rate in order to investigate the effect of pressure changes in the pipeline on the internal states of the MH tank. In addition, the sensitivity analysis of selected unknown parameters in the model has been carried out with the aim of exploring whether reference values from literature can be used in the modified model proposed in this paper. The unknown parameters in the model are identified by the PSO algorithm, and the comparison of simulation and experimental data verifies the validity

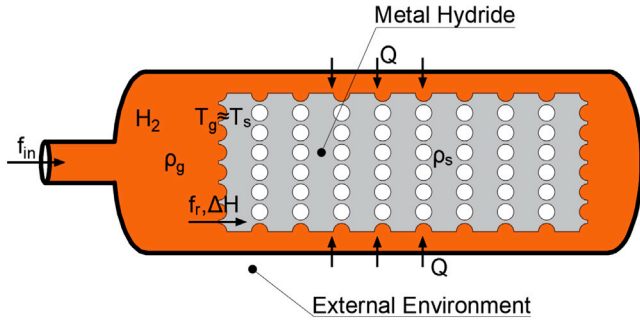


Fig. 1. Schematic of an MH tank (the process of charge).  
Source: Adaptation of [21].

of the proposed model. The model proposed in this paper can be used for observer design to estimate the density of MH solid and hydrogen, especially it can be used to estimate the state of charge (SOC) of the storage tank.

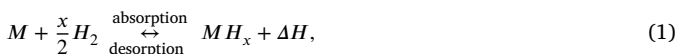
The main contributions of this paper can be summarized as follows:

1. A two-dimensional state-space model of MH tanks is proposed in which a scenario with pipe pressure as the input variable is considered.
2. Sensitivity analysis method First-order Trajectory Sensitivity Analysis (FOTSA) is used to analyze the sensitivity of the parameters from the proposed model.
3. PSO is used to tune the unknown parameters in the model to fit the experimental data.
4. The validation of the proposed model is verified through experiments.

The paper is organized as follows: Section 2 describes the structure of a typical MH storage tank (without external cooling circulation), together with a description of the reaction processes occurring in the tank during the charge and discharge. Section 3 presents a reduced-order model and a reduced-order modified model of the MH tank. In Section 4, the FOTSA method is used for the reduced-order modified model. Section 5 calibrates the reduced-order modified model based on experimental data. Finally, the conclusions and future work are provided in Section 6.

## 2. System description of the MH tank

The schematic of the MH tank is shown in Fig. 1. The whole MH tank consists of two components: the tank and the metal alloy. For the charging process, hydrogen is introduced into the tank at a specified flow rate. Given that the tank constitutes a confined environment, the influx of hydrogen induces an elevation in pressure. After exceeding the equilibrium pressure, the hydrogen starts to react with the metal alloy to form the MH. This reaction is exothermic and when the tank temperature is higher than the ambient temperature, heat exchange between the external environment and the tank is accelerated, allowing the reaction inside the tank to continue. For the discharging process, the hydrogen flows out of the tank at a specified flow rate and the pressure inside the tank decreases. When the pressure falls below the equilibrium pressure, the MH starts to release hydrogen. This reaction is endothermic and when the tank temperature is lower than the ambient temperature, similarly, heat exchange between the external environment and the tank allows the reaction inside the tank to continue. [22]. The chemical equation of the absorption and desorption process is [23]



where  $M$  is the metal alloy,  $MH_x$  is the MH and  $\Delta H$  is the heat of reaction.

## 3. Model of the MH tank

To build the model of the MH tank, the following assumptions are used in most of the literature:

- The hydrogen gas inside the storage tank is considered an ideal gas [21,24].
- Ignore the thermal convection and thermal radiation inside the tank [21].
- The hydrogen gas and MH satisfy local thermal equilibrium [24].
- Heat transfer from the external environment has a constant heat transfer coefficient [21].
- The volume of the MH remains constant during absorption and desorption [21]. In other words, the volume available for the gas phase remains constant.

In previous literature [21], a three-dimensional state-space model of the MH tank was proposed, which took the temperature  $T$  of the MH tank as a system state and considered the effect of the external cooling circulation. This model is suitable for the thermal management of the MH tank, but it is slightly complex for cases where the heat exchange between the tank and the external environment does not need to be considered. In this section, the model presented in [21] is simplified and then it is modified based on the inputs of the experimental setup.

### Reduced-order model

A reduced-order model of the MH tank is proposed which considers the tank temperature as a system input:

$$\dot{\tilde{x}} = \begin{bmatrix} \frac{\tilde{u}_2 - f_r}{V_g} \\ \frac{f_r}{V_s} \end{bmatrix}, \quad (2)$$

$$\tilde{y} = \tilde{x}_1 \frac{\tilde{u}_1 R}{M_{H_2}}, \quad (3)$$

where

$$\tilde{x} = \begin{bmatrix} \tilde{x}_1 \\ \tilde{x}_2 \end{bmatrix} = \begin{bmatrix} \rho_g \\ \rho_s \end{bmatrix}, \quad \tilde{u} = \begin{bmatrix} \tilde{u}_1 \\ \tilde{u}_2 \end{bmatrix} = \begin{bmatrix} T \\ f_{in} \end{bmatrix}, \quad \tilde{y} = P \quad (4)$$

are the states, inputs and output of the system, respectively. In this model,  $\rho_g$  is the density of hydrogen,  $\rho_s$  is the density of the MH,  $T$  is the temperature of MH,  $f_{in}$  is the normalized mass flow rate of hydrogen,  $P$  is the pressure of hydrogen,  $f_r$  is the normalized sorption mass flow rate of hydrogen,  $R$  is universal gas constant and  $M_{H_2}$  is the molar mass of hydrogen.

$$V_g = \frac{V_{tank}}{V_{MH}} - 1 + \epsilon \quad (5)$$

is the normalized volume of hydrogen,  $V_{tank}$  is the volume of the MH tank,  $V_{MH}$  is the volume of MH and  $\epsilon$  is the porosity of MH.

$$V_s = 1 - \epsilon \quad (6)$$

is the normalized volume of the MH.

The sorption kinetic model is [8,9]:

$$f_r = \begin{cases} C_a e^{-\frac{E_a}{R\tilde{u}_1}} \ln\left(\frac{\tilde{y}}{P_{eq,a}}\right) (\rho_{ss} - \tilde{x}_2), & \tilde{y} > P_{eq,a}, \\ C_d e^{-\frac{E_d}{R\tilde{u}_1}} \left(\frac{\tilde{y} - P_{eq,d}}{P_{eq,d}}\right) (\tilde{x}_2 - \rho_{s0}), & \tilde{y} < P_{eq,d}, \\ 0, & \text{otherwise,} \end{cases} \quad (7)$$

where  $C_a$  and  $C_d$  are the absorption and desorption constants,  $E_a$  and  $E_d$  are the activation energy for absorption and desorption.  $P_{eq,a}$  and  $P_{eq,d}$  are the equilibrium pressure for absorption and desorption, respectively.  $\rho_{ss}$  is the saturated density of the MH with complete absorption of hydrogen and  $\rho_{s0}$  is the empty density of the MH without any hydrogen.

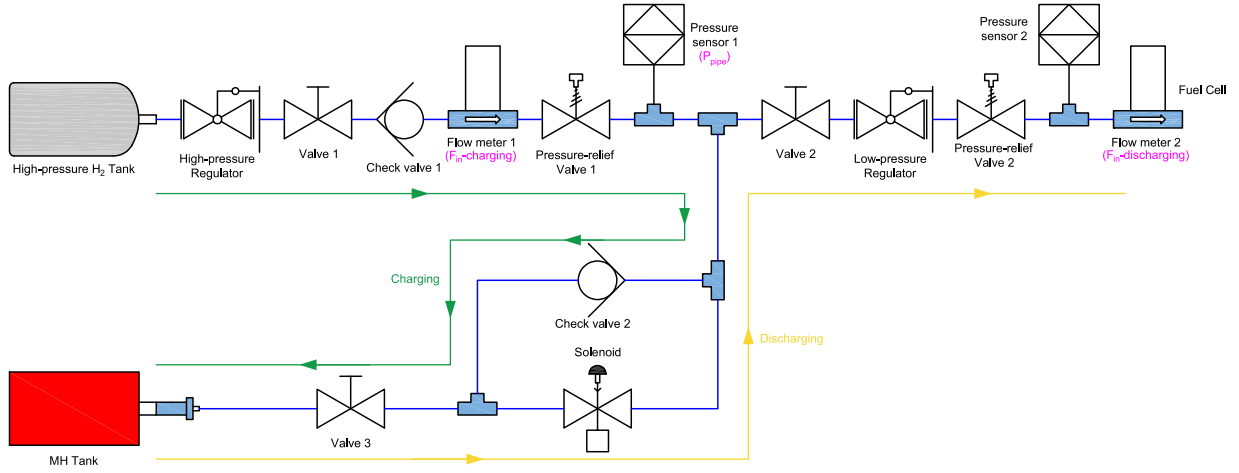


Fig. 2. Schematic diagram of hydrogen circuit.

Equilibrium pressures can be expressed as [22]:

$$P_{eq,a} = P_0 \cdot e^{\left( \frac{\Delta S_d}{R} - \frac{\Delta H_d}{R u_1} + (\varphi + \varphi_0) \tan \left[ \pi \left( \frac{x_2 - \rho_{s0}}{\rho_{ss} - \rho_{s0}} - 0.5 \right) \right] + \frac{\beta}{2} \right)}, \quad (8)$$

$$P_{eq,d} = P_0 \cdot e^{\left( \frac{\Delta S_d}{R} - \frac{\Delta H_d}{R u_1} + (\varphi - \varphi_0) \tan \left[ \pi \left( \frac{x_2 - \rho_{s0}}{\rho_{ss} - \rho_{s0}} - 0.5 \right) \right] - \frac{\beta}{2} \right)}. \quad (9)$$

where  $\Delta H_d$  is the enthalpy change for desorption,  $\Delta S_d$  is the entropy change for desorption,  $P_0$  is the atmospheric pressure,  $\varphi$  and  $\varphi_0$  are the plateau flatness coefficients and  $\beta$  is the plateau hysteresis coefficient.

**Remark 1.** Heat is generated and consumed by the alloy as it absorbs and desorbs hydrogen, which can cause differences in temperature between the inside and outside of the tank in a short time. Consequently, the temperature measured by the thermocouple located outside the tank may not accurately reflect the temperature within it. However, it is possible to approximate the temperature measured outside the tank as the internal temperature if the heat transfer coefficient of the material of the tank's external walls is sufficiently large or the effects of the tank walls are just neglected. Then, the temperature  $T$  inside the tank can be regarded as a measurable variable.

#### Reduced-order modified model

In two-dimensional MH tank model (2) and (3), the normalized mass flow rate  $f_{in}$  is the model input and the pressure  $P$  is the model output. However, in experimental operations, to ensure safety and prevent the pressure inside the tank from exceeding the limit pressure of the MH tank, the pressure at the entrance of the MH tank is sometimes changed by tuning the pressure regulator and using the pipe pressure  $P_{pipe}$  as the model input. This is the case for the experimental setup we developed.

Fig. 2 shows the hydrogen circuit of our MH tank test bench. The pipe pressure is controlled by rotating the high-pressure regulator at the outlet of the high-pressure hydrogen storage tank for charging and discharging operations.

In our case, the model output is normalized mass flow rate  $f_{in}$ . However, due to the model's complexity and the strong coupling between pressure and other parameters, inverting the normalized mass flow rate by pressure is challenging. Based on this, to avoid large changes to the existing model, one method is to convert the input and output of the model through the pipe model, i.e. converting the output of the original model pressure  $P$  into normalized mass flow rate  $f_{in}$ . The diagram for the modification of the model input and output via the pipe model is shown in Fig. 3.

In Fig. 3,  $P_{dif} = P_{pipe} - P$  is the pressure difference between the pressure inside of the MH tank and pipe pressure. When the pressures on the two sides of the entrance of the MH tank are different, the

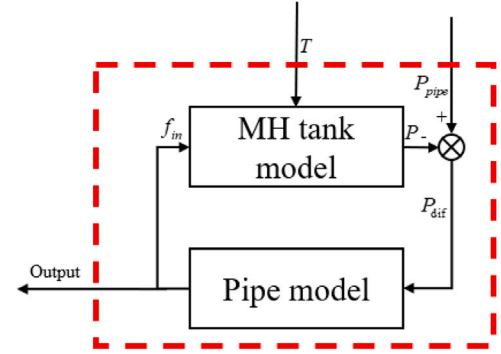


Fig. 3. Modification of model input and output.

pressure difference drives the flow of hydrogen from the side with the higher pressure to the side with the lower pressure. Consider the simplest proportional pipe model to reflect this relationship, i.e. when the normalized mass flow rate is proportional to the pressure difference:

$$f_{in} = k_p \cdot P_{dif} \cdot 10^{-5}, \quad (10)$$

where  $k_p$  is the proportionality coefficient. Then the modified system can be expressed as:

$$\dot{\mathbf{x}} = \begin{bmatrix} k_p \cdot (u_2 - \frac{x_1 u_1 R}{M_{H_2}}) \cdot 10^{-5} - f_r \\ \frac{V_g}{f_r} \\ \frac{V_s}{V_s} \end{bmatrix}, \quad (11)$$

$$y = k_p \cdot (u_2 - \frac{x_1 u_1 R}{M_{H_2}}) \cdot 10^{-5}, \quad (12)$$

where

$$\mathbf{x} = \begin{bmatrix} x_1 \\ x_2 \end{bmatrix} = \begin{bmatrix} \rho_g \\ \rho_s \end{bmatrix}, \mathbf{u} = \begin{bmatrix} u_1 \\ u_2 \end{bmatrix} = \begin{bmatrix} T \\ P_{pipe} \end{bmatrix}, y = f_{in} \quad (13)$$

are the states, inputs and output of the system, respectively.

The expression of sorption kinetic  $f_r$  and equilibrium pressure  $P_{eq}$  in this model have the same form as the expression in the reduced order model and will not be repeated here.

#### 4. Sensitivity analysis of the MH tank

As shown in the previous section, the state-space model of the MH tank contains a large number of unknown parameters. Before the

model can be used for subsequent studies, it must be calibrated using experimental data. The values of some parameters in the model, such as enthalpy change, entropy change and other variables are related to the materials inside the MH tank, and different values can be found in the relevant literature depending on the materials used. However, the published values of these parameters in the literature were obtained under different operating conditions, and using these parameter values in the model directly may prevent the calibrated model from providing a good fit to the experimental data. Therefore, it is crucial to determine which parameters in the model have a large impact on the system dynamics. For those parameters that have a large impact, it is not feasible to use values from the literature directly. To determine the sensitivity of the parameters in the model, sensitivity analysis is required.

#### 4.1. First-order trajectory sensitivity analysis

Inspired by recent works [25], the FOTSA method is used to analyze the sensitivity of parameters in the reduced-order modified model. Compared to other sensitivity analysis methods (e.g. Multi-Parametric Sensitivity Analysis (MPSA) [26,27]), FOTSA has lower computational costs.

Consider the dynamic system defined by:

$$\dot{\mathbf{x}} = \mathbf{f}(\mathbf{x}, \mathbf{u}, \theta), \quad (14)$$

$$\mathbf{y} = \mathbf{h}(\mathbf{x}, \mathbf{u}, \theta), \quad (15)$$

where  $\mathbf{x} \in \mathbb{R}^n$  denotes the state vector;  $\mathbf{u} \in \mathbb{R}^m$  is the input vector;  $\theta = [\theta_k, \theta_u]$  is a constant parameter vector which contains the known parameter vector  $\theta_k \in \mathbb{R}^{p_1}$  and unknown parameter vector  $\theta_u \in \mathbb{R}^{p_2}$ ;  $\mathbf{f} \in \mathbb{R}^n$  is the vector field and  $\mathbf{h} \in \mathbb{R}^l$  is the output function.

The solutions of (14)–(15),  $\mathcal{X}(t, t_0, \mathbf{x}_{t_0}, \mathbf{u}, \theta)$ , are curves which depend on the parameters,  $\theta$ , the exogenous inputs,  $\mathbf{u}$ , in the interval  $t \in [t_0, t_d]$ , and the initial conditions  $\mathbf{x}_{t_0} \triangleq \mathbf{x}(t_0)$ . These solutions fulfill

$$\frac{\partial \mathcal{X}(t, t_0, \mathbf{x}_{t_0}, \mathbf{u}, \theta)}{\partial t} = \mathbf{f}(\mathcal{X}(t, t_0, \mathbf{x}_{t_0}, \mathbf{u}, \theta), \mathbf{u}(t), \theta) \quad (16)$$

for all time  $t \in [t_0, t_d]$ .

The sensitivity of a solution  $\mathcal{X}(t, t_0, \mathbf{x}_{t_0}, \mathbf{u}, \theta)$ , regarding the unknown parameters  $\theta_u$  can be defined as

$$\frac{\partial \mathcal{X}(t, t_0, \mathbf{x}_{t_0}, \mathbf{u}, \theta)}{\partial \theta_u} \in \mathbb{R}^{n \times p_2}, \quad (17)$$

which indicates the effect of slight variations in the unknown parameters  $\theta_u$  on the solution trajectory.

For simplicity, define  $\dot{\mathcal{X}} \triangleq \frac{\partial \mathcal{X}(t, t_0, \mathbf{x}_{t_0}, \mathbf{u}, \theta)}{\partial t}$  and  $\mathcal{X} \triangleq \mathcal{X}(t, t_0, \mathbf{x}_{t_0}, \mathbf{u}, \theta)$ . The sensitivity of the derivative of the solution can be computed as

$$\frac{\partial \dot{\mathcal{X}}}{\partial \theta_u} = \frac{\partial \mathbf{f}}{\partial \mathcal{X}} \cdot \frac{\partial \mathcal{X}}{\partial \theta_u} + \frac{\partial \mathbf{f}}{\partial \mathbf{u}} \cdot \frac{\partial \mathbf{u}}{\partial \theta_u} + \frac{\partial \mathbf{f}}{\partial \theta_u}. \quad (18)$$

Under the assumption that  $\mathbf{u}$  is an exogenous signal, it can be stated that it is independent of the system unknown parameters  $\theta_u$ , so

$$\frac{\partial \mathbf{u}}{\partial \theta_u} = \mathbf{0} \in \mathbb{R}^{m \times p_2}. \quad (19)$$

Consequently, Eq. (18) can be simplified to

$$\frac{\partial \dot{\mathcal{X}}}{\partial \theta_u} = \frac{\partial \mathbf{f}}{\partial \mathcal{X}} \cdot \frac{\partial \mathcal{X}}{\partial \theta_u} + \frac{\partial \mathbf{f}}{\partial \theta_u}. \quad (20)$$

Note that  $\frac{\partial \dot{\mathcal{X}}}{\partial \theta_u} = \frac{\partial}{\partial \theta_u} \left( \frac{\partial \mathcal{X}}{\partial t} \right)$  and define the First-order Trajectory Sensitivity Function (FOTSF) as

$$\lambda \triangleq \frac{\partial \dot{\mathcal{X}}}{\partial \theta_u} \in \mathbb{R}^{n \times p_2}, \quad (21)$$

it can be stated that

$$\lambda = \frac{\partial \mathbf{f}}{\partial \mathbf{x}} \lambda + \frac{\partial \mathbf{f}}{\partial \theta_u}. \quad (22)$$

At time  $t = t_0$ ,  $\mathcal{X} = \mathbf{x}_{t_0}$ , which is assumed independent of  $\theta$ . Consequently  $\lambda(t_0) = \mathbf{0}$ .

To compute Eq. (22), the information of  $\mathbf{x}$  and  $\mathbf{u}$  is necessary, so Eq. (14) must be solved simultaneously to obtain the current state information.

To quantify the variations in system states caused by the variations in the system unknown parameters  $\Delta \theta_u$ , Eq. (14) is approximated by a first-order Taylor expansion, which is expressed as follows:

$$\mathcal{X}(\theta_u + \Delta \theta_u) = \mathcal{X}(\theta_u) + \left( \frac{\partial \mathcal{X}(\theta_u)}{\partial \theta_u} \right) \cdot \Delta \theta_u + o(\theta_u). \quad (23)$$

Substituting Eq. (21) into Eq. (23) and defining  $\Delta \mathcal{X} \triangleq \mathcal{X}(\theta_u + \Delta \theta_u) - \mathcal{X}(\theta_u)$ , it can be shown that

$$\Delta \mathcal{X} = \lambda \cdot \Delta \theta_u + o(\theta_u), \quad (24)$$

where  $o(\theta_u)$  is the Taylor residual.

Each state variation caused by a single parameter variation is

$$\Delta \mathcal{X}_i = \lambda_{i,j} \cdot \Delta \theta_j + o(\theta_u), \quad (25)$$

where  $i = 1, 2, \dots, n$  is the component of the states and  $j = 1, 2, \dots, p_2$  is the component of sensitivity and parameters.

The maximum absolute value of each  $\Delta \mathcal{X}_i$  under the same percentage of  $\Delta \theta_j$  during  $t \in [t_0, t_d]$  is chosen as the sensitivity index  $s_i$ , which can be expressed as:

$$s_i = \max |\Delta \mathcal{X}_i|. \quad (26)$$

---

#### Algorithm 1: FOTSA of the modified MH tank model

---

**Input** : Pipe pressure  $P_{pipe}$ , Temperature  $T$  of the MH tank

**1 Initialization:**

- Set the initial value of the hydrogen and metal-hydride density  $\rho_g(t_0)$ ,  $\rho_s(t_0)$ , initial value of sensitivity function  $\lambda(t_0)$
- Set the prespecified parameter values (either nominal or actual estimates) of each parameter  $\theta_j$
- Set the sampling interval  $\Delta t$  and the stop time  $t_d$

**2 Start procedure;**

**3 while**  $t \leq t_d$  **do**

- 4     Compute the coefficient items matrix ( $\partial \mathbf{f} / \partial \mathbf{x}$ ) and free items matrix ( $\partial \mathbf{f} / \partial \theta_u$ );
- 5     Compute the sensitivity function  $\lambda$  by Eq. (22);
- 6     Compute each state variation  $\Delta \mathcal{X}_i$  caused by single parameter variation via Eq. (25);
- 7     Compute the sensitivity index  $s_i$  of each parameter by Eq. (26);

**8 end**

**9 End procedure;**

**Output:** Sensitivity index  $s_i$

---

The FOTSA method for the MH tank is presented in Algorithm 1. Through a comparison of the sensitivity index for each parameter, it is feasible to discern the impact of minor variations in individual parameters on the system's trajectories. It is important to highlight that a higher sensitivity index corresponds to a more significant influence on the system's trajectories. Conversely, a lower sensitivity index indicates a relatively smaller effect.

#### 4.2. Sensitivity analysis of the reduced-order modified MH tank model

To facilitate the sensitivity analysis, three operating conditions are defined, corresponding to the charge, discharge and mixed charge &

**Table 1**  
Prespecified values of parameters [29–33].

Parameter	Symbol	Prespecified value	Unit
Entropy change for desorption	$\Delta S_d$	111.77	J/mol/K
Enthalpy change for desorption	$\Delta H_d$	$2.668 \cdot 10^4$	J/mol
Plateau flatness coefficient	$\varphi$	0.1843	–
Plateau flatness coefficient	$\varphi_0$	0.0042	–
Plateau hysteresis coefficient	$\beta$	0.2355	–
Absorption constant	$C_a$	3928.1	1/s
Desorption constant	$C_d$	4952.2	1/s
Activation energy for absorption	$E_a$	$3.8236 \cdot 10^4$	J/mol
Activation energy for desorption	$E_d$	$3.0915 \cdot 10^4$	J/mol

**Table 2**  
Other parameters used in the MH tank model [21].

Symbol	Value	Symbol	Value
$\epsilon$	0.6997	$V_{MH}$	$0.353 \cdot 10^{-3} \text{m}^3$
$\rho_{s0}$	6211.1 kg/m <sup>3</sup>	$\rho_{H_2}$	0.0897 kg/m <sup>3</sup>
$R$	8.314 J/(mol K)	$P_0$	101 325 Pa
$M_{H_2}$	$2.016 \cdot 10^{-3} \text{kg/mol}$	$T_{amb}$	298.15 K
$V_{tank}$	$0.48 \cdot 10^{-3} \text{m}^3$	$k_p$	0.06 s/m
$V_{H_2}$	0.35 m <sup>3</sup>	$k_{amb}$	0.7 J/(s K)
$C_{pg}$	14 890 J/(kg K)	$C_{ps}$	400 J/(kg K)

discharge conditions of the MH tank. Since temperature is considered a measurable variable in the reduced-order model, the third-order model is used to generate temperature data. The expression of temperature is [28]:

$$\dot{T} = \frac{f_r \frac{\Delta H}{M_{H_2}} + f_r T (C_{pg} - C_{ps}) + Q}{V_g C_{pg} \rho_g + V_s C_{ps} \rho_s}, \quad (27)$$

where  $C_{pg}$  and  $C_{ps}$  are the specific heat of hydrogen and MH, respectively.

The heat exchange per unit volume,  $Q$ , with the ambient air and the MH tank can be computed as

$$Q = \frac{k_{amb} \cdot (T_{amb} - T)}{V_{MH}}, \quad (28)$$

where  $k_{amb}$  is the overall heat exchange coefficient between the ambient air and the MH tank, and  $T_{amb}$  is the ambient temperature.

In the reduced-order modified model proposed in the above section, the unknown parameter vector is  $\theta_u = [\Delta S_d, \Delta H_d, \varphi, \varphi_0, \beta, C_a, C_d, E_a, E_d, \epsilon, \rho_{s0}, \rho_{si}, V_{MH}, k_p]$ . Since the three parameters  $V_{MH}$ ,  $\epsilon$ ,  $\rho_{s0}$  are related to the manufacturing techniques of the MH inside the tanks,  $\rho_{si}$  is the initial state which cannot calculate directly and  $k_p$  have a large influence on the flow of hydrogen, it is necessary to fix these five parameters during the model calibration. Then, for the sensitivity analysis, the following nine parameters are selected:  $\theta_s = [\Delta S_d, \Delta H_d, \varphi, \varphi_0, \beta, C_a, C_d, E_a, E_d] \subset \theta_u$ . The prespecified values of unknown parameters  $\theta_s$  used for sensitivity analysis are shown in Table 1. Other parameters used in the model are listed in Table 2.

### Charging process

The first operating condition is charge. In the reduced-order modified model (11)–(12), the input variable is pipe pressure, so a stepped pipe pressure profile is defined. To make the initial state of the tank model equilibrium, the initial conditions of the pipe pressure profile are defined as  $\rho_g(t_0) = 0.0813 \text{ kg/m}^3$ ,  $\rho_s(t_0) = 6217.5 \text{ kg/m}^3$  and  $P_{pipe}(t_0) = 0.1 \text{ MPa}$ . The pipe pressure increases by 0.1 MPa every 2000 s until the reference pressure  $P_{ref} = 2.5 \text{ MPa}$ . Fig. 4 shows the system dynamics for the charging process.

The evolution of  $\lambda_{i,j}$  for  $\rho_g$  in charge condition is shown in Fig. 5. From the figure, it can be found that under this operating condition, five parameters:  $\Delta S_d$ ,  $\Delta H_d$ ,  $\beta$ ,  $C_a$  and  $E_a$  have sustainable effects on the dynamic performance of the system state  $\rho_g$  while  $\varphi$  and  $\varphi_0$  only have effect at the beginning of the charging process. Besides, it can be noted that the changes of both  $C_d$  and  $E_d$  have no effect on  $\rho_g$  because the

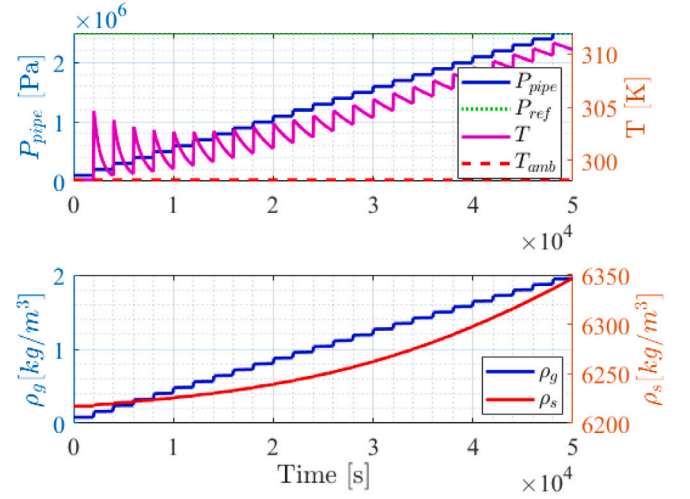


**Fig. 4.** The charge profile of sensitivity analysis.

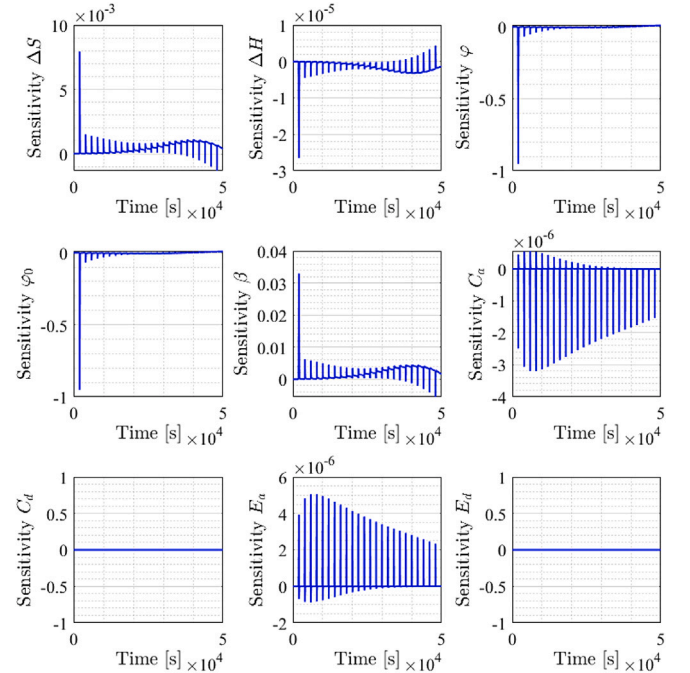


**Fig. 5.** Parameter sensitivity function for  $\rho_g$  of charging process.

trajectories of these two parameters' sensitivity functions are always 0. This is reasonable as the charging process does not include information related to these two parameters.

The numeric variation for each parameter is set as 3% of their prespecified values for the sensitivity analysis of  $\rho_g$ . The result of the sensitivity index for  $\rho_g$  is shown in Table 3. From this table, it can be observed intuitively that the four parameters  $\Delta S_d$ ,  $\Delta H_d$ ,  $E_a$  and  $\varphi$  have more impact on system state  $\rho_g$ , and sensitivities, in descending order, are  $\Delta S_d > \Delta H_d > E_a > \varphi$ .

The evolution of  $\lambda_{i,j}$  for  $\rho_s$  in charge condition is shown in Fig. 6. Similarly, it can be observed that  $C_d$  and  $E_d$  do not affect  $\rho_s$ .

Next, the numeric variation for each parameter is set as 3% of their prespecified values for the sensitivity analysis of  $\rho_s$ . The result of the sensitivity index for  $\rho_s$  is shown in Table 4. This table shows that the five parameters  $\Delta S_d$ ,  $\Delta H_d$ ,  $E_a$ ,  $\varphi$  and  $\beta$  have more impact on system state  $\rho_s$ , and sensitivities, in descending order, are  $\Delta S_d > \Delta H_d > \beta > E_a > \varphi$ .

**Table 3**  
Sensitivity index for  $\rho_g$  of charging process with 3% parameter variation.

Parameter	Symbol	$s_1(3\%)$
Entropy change for desorption	$\Delta S_d$	0.0266
Enthalpy change for desorption	$\Delta H_d$	0.0212
Plateau flatness coefficient	$\varphi$	0.0053
Plateau flatness coefficient	$\varphi_0$	$1.1983 \cdot 10^{-4}$
Plateau hysteresis coefficient	$\beta$	$2.3287 \cdot 10^{-4}$
Absorption constant	$C_a$	$3.7734 \cdot 10^{-4}$
Desorption constant	$C_d$	-
Activation energy for absorption	$E_a$	0.0058
Activation energy for desorption	$E_d$	-

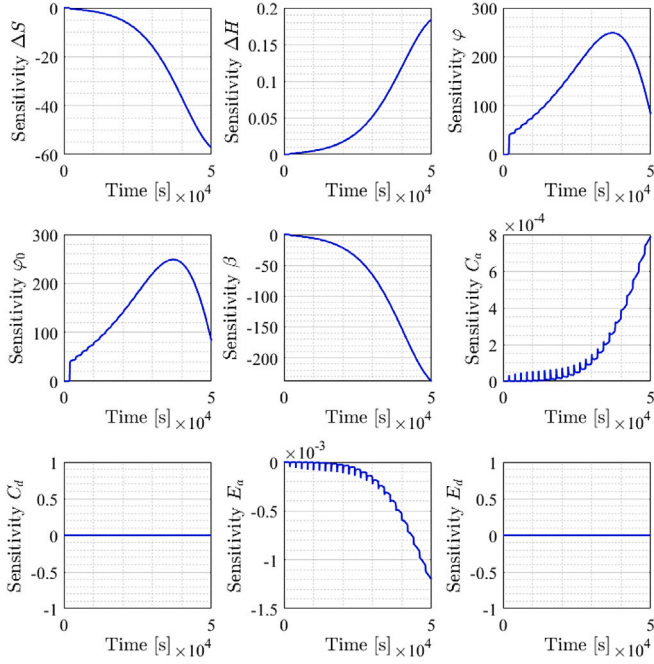


**Fig. 6.** Parameter sensitivity function for  $\rho_s$  of charging process.

**Table 4**  
Sensitivity index for  $\rho_s$  of charging process with 3% parameter variation.

Parameter	Symbol	$s_2(3\%)$
Entropy change for desorption	$\Delta S_d$	191.8114
Enthalpy change for desorption	$\Delta H_d$	147.4213
Plateau flatness coefficient	$\varphi$	1.3757
Plateau flatness coefficient	$\varphi_0$	0.0314
Plateau hysteresis coefficient	$\beta$	1.6801
Absorption constant	$C_a$	0.0930
Desorption constant	$C_d$	-
Activation energy for absorption	$E_a$	1.3772
Activation energy for desorption	$E_d$	-

Therefore, in cases where charge experimental data is accessible, it is even more important to determine reasonable ranges for the five parameters  $\Delta S_d$ ,  $\Delta H_d$ ,  $\varphi$ ,  $\beta$  and  $E_a$  in model calibration. Compared to these five parameters, the remaining four parameters have less effect on system states. When precise results are not required, calibration of the important parameters should be prioritized, while prespecified values can be used for other parameters to reduce the number of calibrated parameters.

#### Discharging process

The second operating condition is discharge. In contrast to the charge, the initial conditions are defined as  $\rho_g(t_0) = 2.0331 \text{ kg/m}^3$ ,  $\rho_s(t_0) = 6481 \text{ kg/m}^3$  and  $P_{pipe}(t_0) = 2.5 \text{ MPa}$ . The pipe pressure decreases

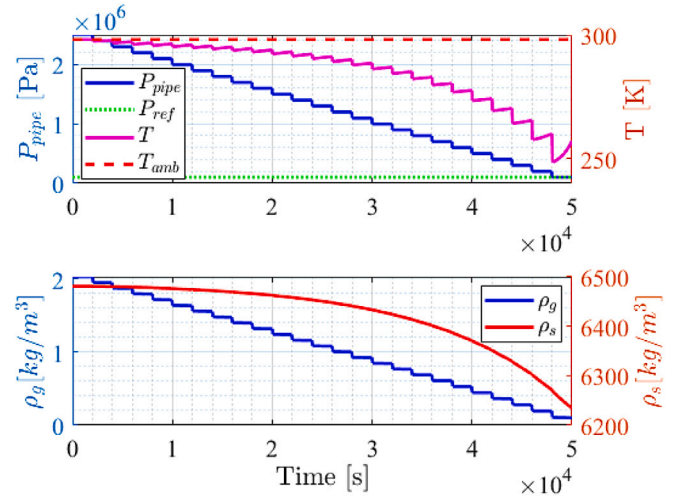


**Fig. 7.** The discharge profile of sensitivity analysis.

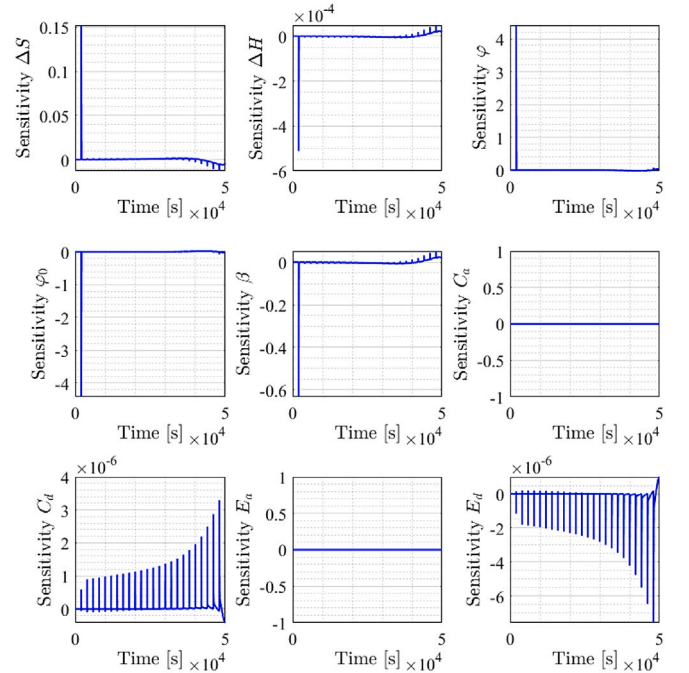


**Fig. 8.** Parameter sensitivity function for  $\rho_g$  of discharging process.

by 0.1 MPa every 2000 s until the reference pressure  $P_{ref} = 0.1 \text{ MPa}$ . Fig. 7 shows the system dynamics for the discharging process.

Figs. 8 and 9 show the evolution of  $\lambda_{i,j}$  for  $\rho_g$  and  $\rho_s$  in discharge condition, respectively. These figures reveal that all the parameters except  $C_a$  and  $E_a$  have significant effects on the dynamic performance of the system states  $\rho_g$  and  $\rho_s$ . The reason is similar to that described earlier, i.e. the information of these two parameters is not included in the discharging process.

The calculation results of the sensitivity index for  $\rho_g$  and  $\rho_s$  are listed in Table 5 and Table 6, respectively. From these two tables, it can be noted that the five parameters  $\Delta S_d$ ,  $\Delta H_d$ ,  $\varphi$ ,  $\beta$  and  $E_d$  have more impact on system state  $\rho_g$ , and sensitivities, in descending order, are  $\Delta S_d > \Delta H_d > \varphi > E_d > \beta$ . In the meanwhile, the five parameters  $\Delta S_d$ ,  $\Delta H_d$ ,  $\varphi$ ,  $\beta$  and  $E_d$  have more impact on system state  $\rho_s$ , and sensitivities, in descending order, are  $\Delta S_d > \Delta H_d > E_d > \beta > \varphi$ .

Hence, in cases where discharge experimental data is available, it is crucial to determine reasonable ranges for the five parameters:  $\Delta S_d$ ,

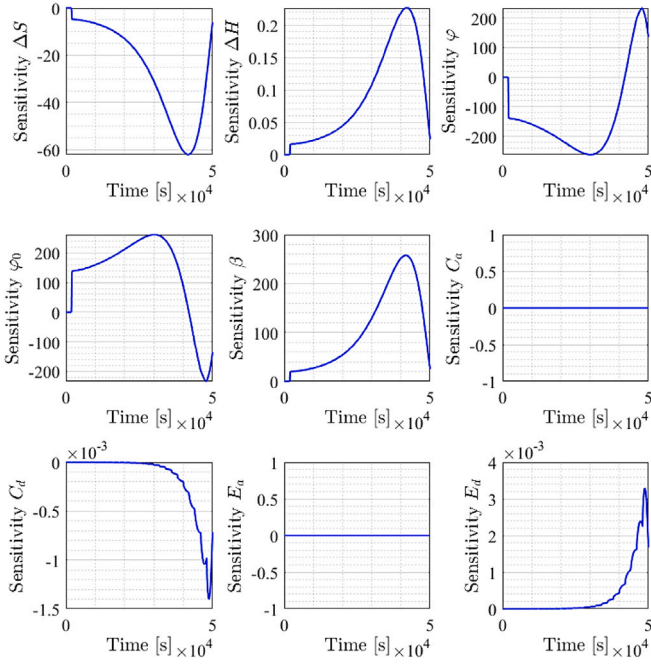


Fig. 9. Parameter sensitivity function for  $\rho_s$  of discharging process.

**Table 5**  
Sensitivity index for  $\rho_g$  of discharging process with 3% parameter variation.

Parameter	Symbol	$s_1(3\%)$
Entropy change for desorption	$\Delta S_d$	0.5104
Enthalpy change for desorption	$\Delta H_d$	0.4089
Plateau flatness coefficient	$\varphi$	0.0244
Plateau flatness coefficient	$\varphi_0$	$5.5682 \cdot 10^{-4}$
Plateau hysteresis coefficient	$\beta$	0.0045
Absorption constant	$C_a$	–
Desorption constant	$C_d$	$4.8855 \cdot 10^{-4}$
Activation energy for absorption	$E_a$	–
Activation energy for desorption	$E_d$	0.0070

**Table 6**  
Sensitivity index for  $\rho_s$  of discharging process with 3% parameter variation.

Parameter	Symbol	$s_2(3\%)$
Entropy change for desorption	$\Delta S_d$	208.0995
Enthalpy change for desorption	$\Delta H_d$	181.2052
Plateau flatness coefficient	$\varphi$	1.4461
Plateau flatness coefficient	$\varphi_0$	0.0330
Plateau hysteresis coefficient	$\beta$	1.8228
Absorption constant	$C_a$	–
Desorption constant	$C_d$	0.2081
Activation energy for absorption	$E_a$	–
Activation energy for desorption	$E_d$	3.0613

$\Delta H_d$ ,  $\varphi$ ,  $\beta$ , and  $E_d$  during model calibration. In comparison to these five parameters, the impact of the remaining four parameters has a relatively less significant effect on the state of the system.

### Mixed charging & discharging process

The third operating condition is the mixed charging & discharging process which contains charge and discharge. The initial conditions are defined as  $\rho_g(t_0) = 0.9759 \text{ kg/m}^3$ ,  $\rho_s(t_0) = 6270 \text{ kg/m}^3$  and  $P_{pipe}(t_0) = 1.2 \text{ MPa}$ . To fully consider the charge and discharge scenarios, an extreme case has been chosen, i.e. pipe pressure is a periodic square wave signal,  $P_{pipe} = 1.2 \text{ MPa}$  while  $t \in [0, 2500 \text{ s}]$ ,  $P_{pipe} = 1.6 \text{ MPa}$  while  $t \in [2500 \text{ s}, 5000 \text{ s}]$ ,  $P_{pipe} = 0.8 \text{ MPa}$  while  $t \in [5000 \text{ s}, 7500 \text{ s}]$ , and then it varies with a period of 2500 s. Fig. 10 shows the system dynamics for the mixed charging & discharging process.

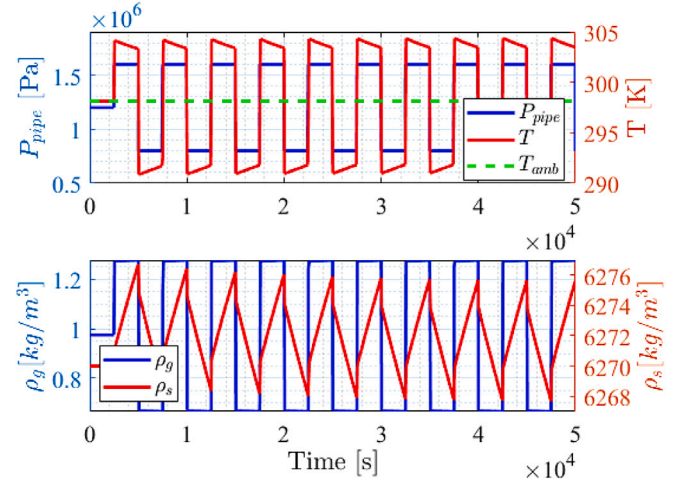


Fig. 10. The mixed charging & discharging profile of sensitivity analysis.

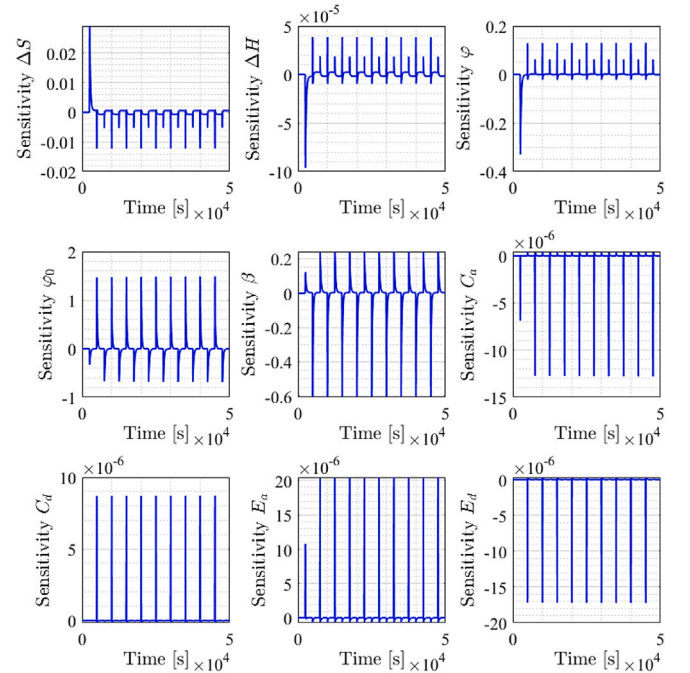


Fig. 11. Parameter sensitivity function for  $\rho_g$  of mixed charging & discharging process.

**Table 7**  
Sensitivity index for  $\rho_g$  of mixed charging & discharging process with 3% parameter variation.

Parameter	Symbol	$s_1(3\%)$
Entropy change for desorption	$\Delta S_d$	0.0979
Enthalpy change for desorption	$\Delta H_d$	0.0770
Plateau flatness coefficient	$\varphi$	0.0018
Plateau flatness coefficient	$\varphi_0$	$1.8826 \cdot 10^{-4}$
Plateau hysteresis coefficient	$\beta$	0.0043
Absorption constant	$C_a$	0.0015
Desorption constant	$C_d$	0.0013
Activation energy for absorption	$E_a$	0.0235
Activation energy for desorption	$E_d$	0.0160

The evolution of  $\lambda_{i,j}$  for  $\rho_g$  and  $\rho_s$  in the mixed charging & discharging process are shown in Figs. 11 and 12, it can be found that all the parameters have significant effects on the dynamic performance of the system state  $\rho_g$  and  $\rho_s$ .

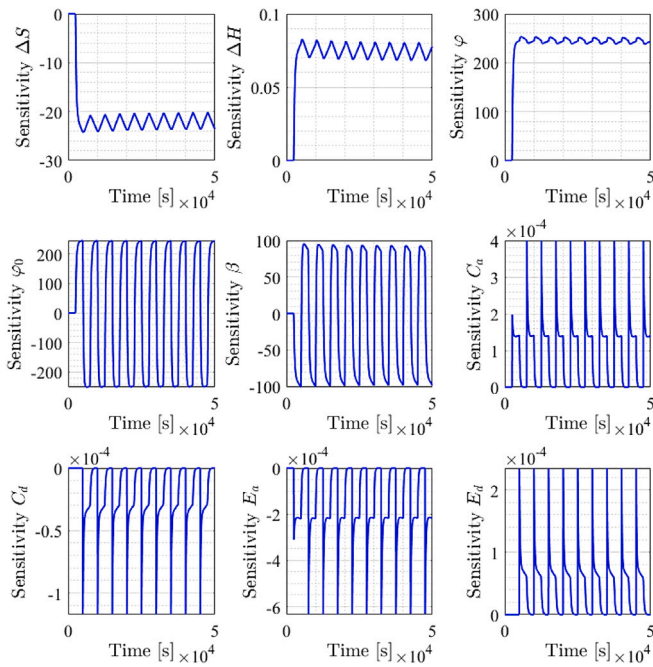


Fig. 12. Parameter sensitivity function for  $\rho_s$  of mixed charging & discharging process.

Table 8

Sensitivity index for  $\rho_s$  of mixed charging & discharging process with 3% parameter variation.

Parameter	Symbol	$s_2(3\%)$
Entropy change for desorption	$\Delta S_d$	81.4803
Enthalpy change for desorption	$\Delta H_d$	66.1727
Plateau flatness coefficient	$\varphi$	1.3985
Plateau flatness coefficient	$\varphi_0$	0.0316
Plateau hysteresis coefficient	$\beta$	0.7122
Absorption constant	$C_a$	0.0472
Desorption constant	$C_d$	0.0174
Activation energy for absorption	$E_a$	0.7284
Activation energy for desorption	$E_d$	0.2180

The results of the sensitivity index for  $\rho_g$  and  $\rho_s$  are listed in Tables 7 and 8. From these two tables, it can be observed intuitively that the five parameters  $\Delta S_d$ ,  $\Delta H_d$ ,  $\beta$ ,  $E_a$  and  $E_d$  have more impact on system state  $\rho_g$ , and sensitivities, in descending order, are  $\Delta S_d > \Delta H_d > E_a > E_d > \beta$ . In the meanwhile, the six parameters  $\Delta S_d$ ,  $\Delta H_d$ ,  $\varphi$ ,  $\beta$ ,  $E_a$  and  $E_d$  have more impact on system state  $\rho_s$ , and sensitivities, in descending order, are  $\Delta S_d > \Delta H_d > \varphi > E_a > \beta > E_d$ .

Therefore, in cases where mixed charging & discharging experimental data is accessible, it is important to determine reasonable ranges for these six parameters:  $\Delta S_d$ ,  $\Delta H_d$ ,  $\varphi$ ,  $\beta$ ,  $E_a$  and  $E_d$  in model calibration. Compared to these six parameters, the remaining three parameters have less effect on system states.

From the results of the sensitivity analysis of the above three processes, it can be seen that both  $\Delta S_d$  and  $\Delta H_d$  have the highest sensitivity. These two parameters, which are important parameters of the standard Van't Hoff equation [7], have a greater influence on the equilibrium pressure than the plateau flatness coefficients and the hysteresis coefficients, thus these two parameters have high sensitivity to the system states  $\rho_g$  and  $\rho_s$ . Meanwhile, the results of the sensitivity analysis simplify the subsequent calibration of the MH model with experimental data. When the MH model is calibrated using experimental data containing only the charging process or only the discharging process, the segmented functions of reaction kinetics  $f_r$  and equilibrium pressure  $P_{eq}$  can be simplified and calculated using the corresponding equations. In addition, the number of parameters in the model that need to be calibrated is also reduced.

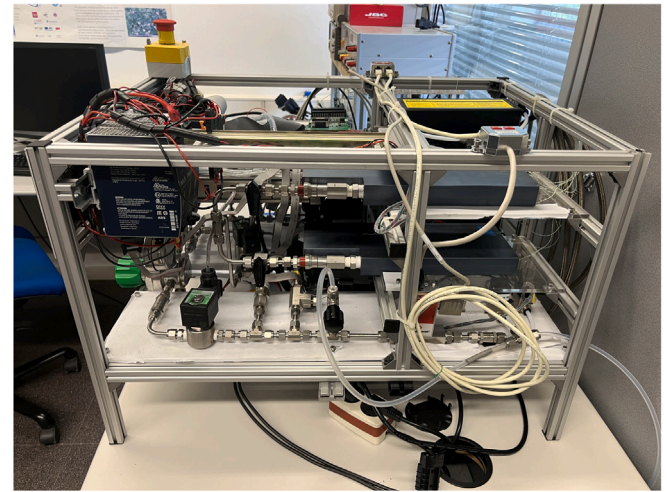


Fig. 13. View of the MH tank test bench.

Table 9

Characteristics of the main sensors.

Sensor	Model	Measure range
Mass flow meter	F-111B	0.16 mLn/min-25 Ln/min
Pressure sensor	PR-21Y	2 bar-30 bar
Thermocouple	K	-75 °C-260 °C

## 5. Model calibration of MH tank from data

The experimental data required for calibration are obtained from the practical MH tank test bench (as shown in Fig. 13). The experimental setup comprises two primary components: the hydrogen circuit and the real-time platform. The schematic diagram of the hydrogen circuit is mentioned in Fig. 2. The real-time platform not shown in the figure is used to record the measurement data of each sensor during the experiment. The hydrogen circuit consists of two paths: the charging path and the discharging path.

In the charging path (valve 1 is open and valve 2 is closed), high-pressure (200 bar) hydrogen is stored within a tank, and the outlet of the tank is connected to a high-pressure regulator which decreases the pressure until a range that the MH tank can work. The pressure of the inlet pipe is regulated using the high-pressure regulator. Check valve 1 is used to prevent hydrogen backflow while flow meter 1 is used to measure the flow rate,  $F_{in}$ . Pressure-relief valve 1 (30 bar) is connected behind flow meter 1 to protect the MH tank and the platform. Pressure sensor 1 is used to measure pipe pressure,  $P_{pipe}$ . The solenoid is closed in the charging process and open in the discharging process.

In the discharging path (valve 1 is closed and valve 2 is open). A low-pressure regulator is used to decrease the pressure to 0.5 bar. The pressure-relief valve 2 (1 bar) is used to protect the fuel cell while pressure sensor 2 is used to measure the pressure in the circuit. After the pressure sensor 2 there is the mass flow meter 2 used to measure the flow rate,  $F_{in}$ .

Table 9 lists the characteristics of the main sensors.

The material of the MH tank used in the experiment is Hydralloy C5 ( $Ti_{0.95}Zr_{0.05}Mn_{1.48}Fe_{0.08}Al_{0.01}$ ), which is a  $AB_2$  type alloy [34]. Four temperature sensors are placed on the top and bottom surfaces of the tanks to measure the temperature of their external surfaces.

The following experiment is performed. In the charging process, the pipe pressure,  $P_{pipe}$ , is increased by approximately 1 bar every 5 min until 21 bar by tuning the high-pressure regulator.

In the discharging process, the normalized mass flow rate  $f_{in}$  is controlled to decrease the pressure slowly by tuning the manual relief valve.

**Table 10**  
Search range of the unknown parameters for MH tank model [29–33].

Parameter	Symbol	Lower	Upper	Unit
Entropy change for desorption	$\Delta S_d$	109	113	J/mol/K
Enthalpy change for desorption	$\Delta H_d$	$2.5 \cdot 10^4$	$3.2 \cdot 10^4$	J/mol
Plateau flatness coefficient	$\varphi$	0	1	–
Plateau flatness coefficient	$\varphi_0$	0	1	–
Plateau hysteresis coefficient	$\beta$	0	2	–
Absorption constant	$C_a$	10	5000	1/s
Desorption constant	$C_d$	10	5000	1/s
Activation energy for absorption	$E_a$	$3 \cdot 10^4$	$5 \cdot 10^4$	J/mol
Activation energy for desorption	$E_d$	$3 \cdot 10^4$	$5 \cdot 10^4$	J/mol
Porosity	$\epsilon$	0.1	0.7	–
Empty density of the MH	$\rho_{s0}$	6200	6400	kg/m <sup>3</sup>
Initial density of the MH	$\rho_{si}$	6200	6760.1	kg/m <sup>3</sup>
Volume of MH	$V_{MH}$	$3 \cdot 10^{-4}$	$4.8 \cdot 10^{-4}$	m <sup>3</sup>
Modification coefficient	$k_p$	0.01	1	–

During this experiment, the evolution of the in temperature,  $T$ , pressure in the pipe,  $P_{pipe}$ , and flow rate,  $F_{in}$ , are recorded by the real-time platform.

The pressure of hydrogen  $P$  is modeled by the ideal gas law:

$$P = \rho_g \frac{TR}{M_{H_2}}, \quad (29)$$

so the initial density of hydrogen  $\rho_g(t_0)$  can be calculated by Eq. (29).

Saturated density  $\rho_{ss}$  can be calculated by

$$\rho_{ss} = \rho_{s0} + \frac{V_{H_2} \cdot \rho_{H_2}}{V_{MH} \cdot (1 - \epsilon)}, \quad (30)$$

where  $V_{H_2}$  is the maximum volume of hydrogen that can be absorbed by the tank, i.e. hydrogen capacity and  $\rho_{H_2}$  is the density of hydrogen in standard state, which is considered a constant.

The chosen optimization algorithm is the PSO algorithm. The PSO system comprises a swarm of particles, each representing a potential solution. These particles traverse the search space with a predetermined velocity, seeking the optimal solution. Each particle updates its position in the search space based on its own experience as well as that of its neighboring particles to find the optimal solution [18]. Before applying the PSO algorithm to search for an optimal solution, the range of unknown parameters needs to be determined by experience or literature to make the final optimal value more reasonable and to reduce the computation cost. Table 10 lists the lower and upper bounds for unknown parameters.

To establish the objective function, the normalized mass flow rate,  $f_{in}$  (kg/m<sup>3</sup>/s), need to be converted to the flow rate  $F_{in}$  (Ln/min):

$$F_{in} = \frac{f_{in} \cdot V_{MH} \cdot 60 \cdot 22.4}{M_{H_2}}, \quad (31)$$

Based on Eq. (10), the model pressure satisfying the experimental data  $P_{exp}$  can be calculated as

$$P_{exp} = P_{pipe} - \frac{f_{in}}{k_p \cdot 10^{-5}}. \quad (32)$$

The evaluation criteria used to construct the objective function is the mean magnitude of relative error (MMRE). Since the variable we control in the charging process is pipe pressure while in the discharging process is flow rate, different models should be used. Therefore, the objective function has two terms and can be defined as follows:

$$F_{MH} = \frac{1}{N_1} \cdot \sum_{t=0}^{t=N_1 \Delta t} \left| \frac{F_{in}(t) - F_{in,exp}(t)}{F_{in,exp}(t)} \right| + \frac{1}{N - N_1} \cdot \sum_{t=(N_1+1)\Delta t}^{t=N \Delta t} \left| \frac{P(t) - P_{exp}(t)}{P_{exp}(t)} \right|, \quad (33)$$

where  $F_{in,exp}$  is the experimental data of flow rate.  $\Delta t$  is the sampling interval,  $N_1$  and  $N$  are the sampling times of the charge and whole experiment, respectively. This cost function corresponds to the two

processes of the experiment: charging and discharging. The first term of the objective function is the mean magnitude of relative error of flow rate and the second one is the mean magnitude of relative error of tank pressure.

It is worth noting that not all parameter combinations, as tuned by PSO within the ranges specified in Table 10, will ensure the smooth operation of the tank model. Some combinations may lead to negative air pressure or density, resulting in simulation interruptions. To avoid this problem, the range of some model parameters is limited in the simulation, and the simulation stops when the model pressure exceeds the range.

Figs. 14 and 15 compare the simulation of the calibrated model and experimental data. In the charging process ( $t \in [0, 3970]$ ), it can be seen that, at the top of the pressure step curve, there exists a discrepancy between the pipe pressure  $P_{pipe}$  and the tank pressure  $P$ , and this pressure difference causes the external gas to flow into the tank, and then the discrepancy decreases rapidly, causing the curve of the flow rate to form a spike. In addition, the model does not fit the experimental data well at the spikes of the flow rate curve. One of the reasons is that the existing model is not accurate enough to reflect rapidly changing dynamics. Another reason is the nonzero response time of the sensors used in the experiment. Fig. 16 shows the comparison of the hydrogen volume entering the tanks and the result of the calibrated model is close to experimental data. From the view of the data, it can be calculated that the simulation errors of flow rate in charge, pressure in discharge and gas volume of the whole process are 39.3%, 7.6% and 16.3% respectively.

To verify the validity of the calibrated model under different operating conditions, another set of experimental data is fitted using the calibrated model. Since the initial density of MH  $\rho_s(t_0)$  is different under various experimental conditions, the initial density needs to be estimated when using the calibrated model.  $\rho_s(t_0)$  can be obtained from the PCT curve based on the initial temperature and pressure:

$$\rho_s(t_0) = (1 + wt) \cdot \rho_{s0}. \quad (34)$$

where  $wt$  (%) is the mass percentage of hydrogen relative to the alloy and it can be obtained from the manufacturer (in our work,  $wt = 0.16\%$ ).

**Remark 2.** It is assumed that the tank is in equilibrium at the initial state, so a rough estimate of the initial density  $\rho_s(t_0)$  can be made using the PCT curve provided by the manufacturer of the tank.

The fitting result is shown in Fig. 17 and the result shows that although the calibrated model does not fit the experimental data perfectly under different operating conditions, in general, the calibrated model can roughly reflect the trend of the flow rate and pressure.

## 6. Conclusions and future work

In this paper, a two-dimensional state-space model is proposed by assuming that the tank temperature can be measured. In order to address the conventional approaches where MH models commonly consider the mass flow rate of hydrogen as the system input and overlook industrial scenarios relying on pipe pressure as the system input, the reduced-order model is modified using a pipe model to obtain a reduced-order modified MH tank model. Through defining three profiles, sensitivity analysis is performed on the obtained reduced-order modified model using the FOTSA method. The results of the sensitivity analysis show that the entropy change for desorption  $\Delta S_d$ , enthalpy change for desorption  $\Delta H_d$ , activation energy for absorption  $E_a$ , activation energy for desorption  $E_d$ , plateau flatness coefficient  $\varphi$  and plateau hysteresis coefficient  $\beta$  exhibit higher sensitivities under conditions involving both charge and discharge. This indicates the necessity of selecting reasonable ranges for these parameters during the model calibration process. Based on the sensitivity analysis, the

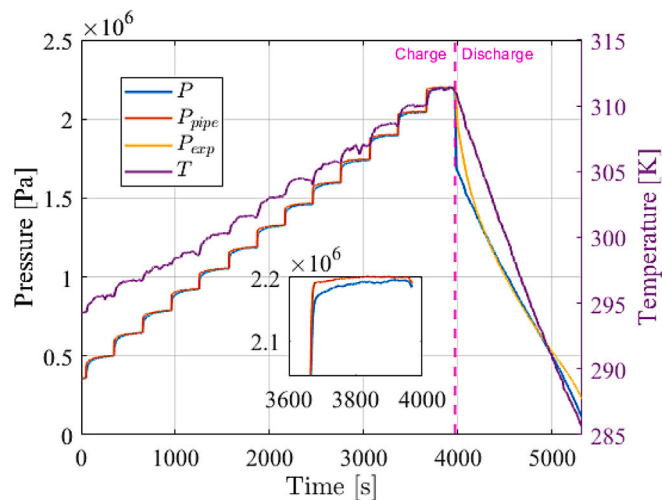


Fig. 14. Comparison of pressure.

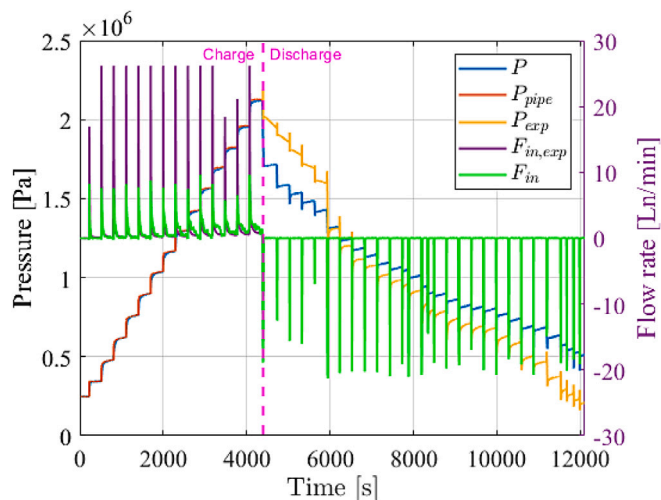


Fig. 17. Fitting with another experiment using calibrated model.

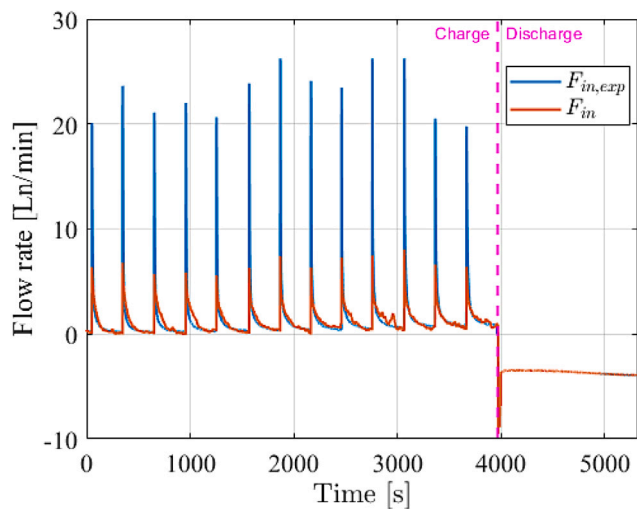


Fig. 15. Comparison of flow rate.

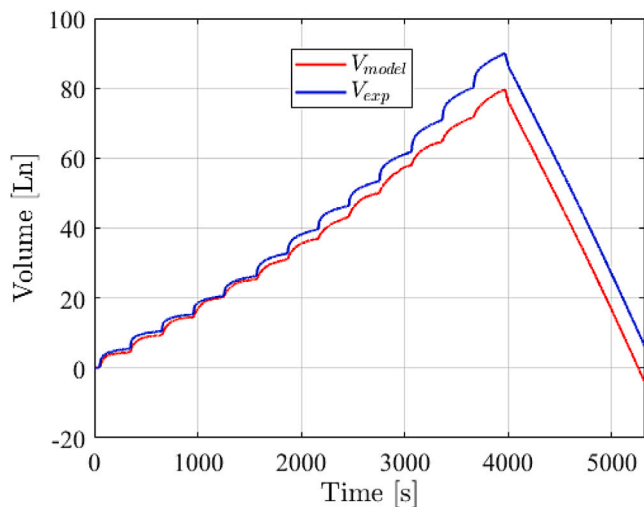


Fig. 16. Comparison of hydrogen volume in tanks.

reduced-order modified model is calibrated in combination with the experimental data. Simulation results of the calibrated model show a good fit to the experimental data and the error of the volume of gas during charge and discharge is 16.7%. Subsequent work will use the calibrated model to estimate the SOC of the MH tank and use a three-dimensional state-space model combined with measured temperatures to determine the Pareto front for multi-objective optimization.

**CRedit authorship contribution statement**

**Mingrui Chen:** Methodology. **Carles Batlle:** Supervision. **Bryan Escachx:** Validation. **Ramon Costa-Castelló:** Project administration. **Jing Na:** Supervision.

**Declaration of competing interest**

The authors declare that they have no known competing financial interests or personal relationships that could have appeared to influence the work reported in this paper.

**Data availability**

Data will be made available on request.

**Acknowledgments**

This work is part of the Project MAFALDA (PID2021-126001OB-C31 funded by MCIN/AEI/10.13039/501100011033 and by “ERDF A way of making Europe”) and Project MASHED (TED2021-129927B-I00 funded by MCIN/AEI/10.13039/501100011033 and by the “European Union Next GenerationEU/PRTR”). This work is partially supported by National Natural Science Foundation of China under grant (62273169) and the Chinese Scholarship Council (CSC) under grant (202208530 009).

**References**

- [1] M.M. Rahman, A.O. Oni, E. Gemechu, A. Kumar, Assessment of energy storage technologies: A review, *Energy Convers. Manage.* 223 (2020) 113295.
- [2] H. Faraji, Ç. Yildiz, A. Arshad, M. Arıcı, K. Choukairy, M. El Alami, Passive thermal management strategy for cooling multiple portable electronic components: Hybrid nanoparticles enhanced phase change materials as an innovative solution, *J. Energy Storage* 70 (2023) 108087.
- [3] K. Im-orb, N. Visitdumrongkul, D. Saebea, Y. Patcharavorachot, A. Arpornwichanop, Flowsheet-based model and exergy analysis of solid oxide electrolysis cells for clean hydrogen production, *J. Cleaner Prod.* 170 (2018) 1–13.

- [4] C. Tarhan, M.A. Çil, A study on hydrogen, the clean energy of the future: Hydrogen storage methods, *J. Energy Storage* 40 (2021) 102676.
- [5] S. Suda, N. Kobayashi, K. Yoshida, Reaction kinetics of metal hydrides and their mixtures, *J. Less Common Metals* 73 (1) (1980) 119–126.
- [6] T. Nishizaki, K. Miyamoto, K. Yoshida, Coefficients of performance of hydride heat pumps, *J. Less Common Metals* 89 (2) (1983) 559–566.
- [7] U. Mayer, M. Groll, W. Supper, Heat and mass transfer in metal hydride reaction beds: experimental and theoretical results, *J. Less Common Metals* 131 (1–2) (1987) 235–244.
- [8] A. Jemni, S.B. Nasrallah, Study of two-dimensional heat and mass transfer during absorption in a metal-hydrogen reactor, *Int. J. Hydrogen Energy* 20 (1) (1995) 43–52.
- [9] A. Jemni, S.B. Nasrallah, Study of two-dimensional heat and mass transfer during desorption in a metal-hydrogen reactor, *Int. J. Hydrogen Energy* 20 (11) (1995) 881–891.
- [10] A. Jemni, S.B. Nasrallah, J. Lamoumi, Experimental and theoretical study of ametal-hydrogen reactor, *Int. J. Hydrogen Energy* 24 (7) (1999) 631–644.
- [11] K. Aldas, M.D. Mat, Y. Kaplan, A three-dimensional mathematical model for absorption in a metal hydride bed, *Int. J. Hydrogen Energy* 27 (10) (2002) 1049–1056.
- [12] M. Stark, G. Krost, D. Lemken, B. Oberschachtsiek, Neural network based modeling of metal-hydride bed storages for small self-sustaining energy supply systems, in: 2011 IEEE Trondheim PowerTech, IEEE, 2011, pp. 1–7, <http://dx.doi.org/10.1109/PTC.2011.6019335>.
- [13] Y. Xing, L. Bernadet, M. Torrell, A. Tarancón, R. Costa-Castelló, J. Na, Offline and online parameter estimation of nonlinear systems: Application to a solid oxide fuel cell system, *ISA Trans.* 133 (2023) 463–474.
- [14] A. Clemente, M. Montiel, F. Barreras, A. Lozano, R. Costa-Castelló, Experimental validation of a vanadium redox flow battery model for state of charge and state of health estimation, *Electrochim. Acta* 449 (2023) 142117.
- [15] M. Kumar, D. Husain, N. Upreti, D. Gupta, et al., Genetic algorithm: Review and application, 2010, Available at SSRN 3529843.
- [16] W. Lee, H.-Y. Kim, Genetic algorithm implementation in python, in: Fourth Annual ACIS International Conference on Computer and Information Science, ICIS'05, IEEE, 2005, pp. 8–11, <http://dx.doi.org/10.1109/ICIS.2005.69>.
- [17] B.C. Mohan, R. Baskaran, A survey: Ant colony optimization based recent research and implementation on several engineering domain, *Expert Syst. Appl.* 39 (4) (2012) 4618–4627.
- [18] R. Thangaraj, M. Pant, A. Abraham, P. Bouvry, Particle swarm optimization: Hybridization perspectives and experimental illustrations, *Appl. Math. Comput.* 217 (12) (2011) 5208–5226.
- [19] D. Zhu, Y. Ait-Amirat, A. N'Diaye, A. Djerdir, New dynamic modeling of a real embedded metal hydride hydrogen storage system, *Int. J. Hydrogen Energy* 44 (55) (2019) 29203–29211.
- [20] S.H. Suárez, D. Chabane, A. N'Diaye, Y. Ait-Amirat, O. Elkedim, A. Djerdir, Evaluation of the performance degradation of a metal hydride tank in a real fuel cell electric vehicle, *Energies* 15 (10) (2022) 3484.
- [21] A.L.J. Keow, A. Mayhall, M. Cescon, Z. Chen, Active disturbance rejection control of metal hydride hydrogen storage, *Int. J. Hydrogen Energy* 46 (1) (2021) 837–851.
- [22] F. Gonzatti, M. Miotto, F. Farret, Automation and analysis of the operation of (La<sub>0.85</sub>Ce<sub>0.15</sub>)Ni<sub>5</sub> in energy storage plants, *Int. J. Hydrogen Energy* 43 (5) (2018) 2850–2860.
- [23] M. Afzal, R. Mane, P. Sharma, Heat transfer techniques in metal hydride hydrogen storage: A review, *Int. J. Hydrogen Energy* 42 (52) (2017) 30661–30682.
- [24] R. Busqué, R. Torres, J. Grau, V. Roda, A. Husar, Mathematical modeling, numerical simulation and experimental comparison of the desorption process in a metal hydride hydrogen storage system, *Int. J. Hydrogen Energy* 43 (35) (2018) 16929–16940.
- [25] X. Kong, K. Ba, B. Yu, Y. Cao, L. Wu, L. Quan, Trajectory sensitivity analysis of first order and second order on position control system of highly integrated valve-controlled cylinder, *J. Mech. Sci. Technol.* 29 (2015) 4445–4464.
- [26] J. Choi, J.W. Harvey, M.H. Conklin, Use of multi-parameter sensitivity analysis to determine relative importance of factors influencing natural attenuation of mining contaminants, in: Proceedings of the Toxic Substances Hydrology Program Meeting, Charleston, SC, 1999, pp. 185–192.
- [27] J.M. Correa, F.A. Farret, V.A. Popov, M.G. Simoes, Sensitivity analysis of the modeling parameters used in simulation of proton exchange membrane fuel cells, *IEEE Trans. Energy Convers.* 20 (1) (2005) 211–218.
- [28] S.B. Nasrallah, A. Jemni, Heat and mass transfer models in metal-hydrogen reactor, *Int. J. Hydrogen Energy* 22 (1) (1997) 67–76.
- [29] M. Kölbig, I. Bürger, M. Linder, Characterization of metal hydrides for thermal applications in vehicles below 0°C, *Int. J. Hydrogen Energy* 44 (10) (2019) 4878–4888.
- [30] J. Barale, F. Nastro, D. Violi, P. Rizzi, C. Luetto, M. Baricco, A metal hydride compressor for a small scale H<sub>2</sub> refuelling station, *Int. J. Hydrogen Energy* (2023).
- [31] G. Capurso, B. Schiavo, J. Jepsen, G. Lozano, O. Metz, A. Saccone, S. De Negri, J.M. Bellosta von Colbe, T. Klassen, M. Dornheim, Development of a modular room-temperature hydride storage system for vehicular applications, *Appl. Phys. A* 122 (2016) 1–11.
- [32] V. Skripnyuk, M. Ron, Evaluation of kinetics by utilizing the normalized pressure dependence method for the alloy Ti<sub>0.95</sub>Zr<sub>0.05</sub>Mn<sub>1.48</sub>V<sub>0.43</sub>Fe<sub>0.08</sub>Al<sub>0.01</sub>, *J. Alloys Compd.* 293 (1999) 385–390.
- [33] C. Chung, C.-S. Lin, Prediction of hydrogen desorption performance of Mg<sub>2</sub>Ni hydride reactors, *Int. J. Hydrogen Energy* 34 (23) (2009) 9409–9423.
- [34] P. Di Giorgio, G. Scarpati, G. Di Ilio, I. Arsie, E. Jannelli, Development of a plug-in fuel cell electric scooter with thermally integrated storage system based on hydrogen in metal hydrides and battery pack, in: E3S Web of Conferences, Vol. 334, EDP Sciences, 2022, p. 06013, <http://dx.doi.org/10.1051/e3sconf/202233406013>.